Production of monodisperse cerium oxide microspheres with diameters near 100 μm by internal-gelation sol–gel methods

Jeffrey A. Katalenich [1,2] · Brian B. Kitchen[1] · Bruce D. Pierson[1]

Abstract

Internal-gelation sol–gel methods have used a variety of sphere-forming methods in the past to produce metal oxide microspheres, but typically with poor control over the size uniformity at diameters near 100 μm. This work describes efforts to make and measure internal-gelation, sol–gel microspheres with very uniform diameters in the 100–200-μm size range using a two-fluid nozzle. A custom apparatus was used to form aqueous droplets of sol–gel feed solutions in silicone oil and heat them to cause gelation of the spheres. Gelled spheres were washed, dried, and sintered prior to mounting them on glass slides for optical imaging and analysis. Microsphere diameters and shape factors were determined as a function of silicone oil flow rate in a two-fluid nozzle and the size of a needle dispensing the aqueous sol–gel solution. Nine batches of microspheres were analyzed and had diameters ranging from 65.5 ± 2.4 μm for the smallest needle and the fastest silicone oil flow rate to 211 ± 4.7 μm for the largest needle and the slowest silicone oil flow rate. Standard deviations for measured diameters were less than 8% for all samples and most of them were less than 4%. Microspheres had excellent circularity with measured shape factors of 0.9–1. However, processing of optical images was complicated by shadow effects in the photoresist layer on glass slides and by overlapping microspheres. Based on the calculated flow parameters, microspheres were produced in a simple dripping mode in the two-fluid nozzle. Using flow rates consistent with a simple dripping mode in a two-fluid nozzle configuration allows for very uniform oxide microspheres to be produced using the internal-gelation sol–gel method.

✉ Jeffrey A. Katalenich
  Jeffrey.Katalenich@pnnl.gov

[1] Department of Nuclear Engineering and Radiological Sciences, University of Michigan, 2355 Bonisteel Blvd., Ann Arbor, MI 48109, USA

[2] Present address: Pacific Northwest National Laboratory, 3230 Innovation Blvd., MSIN K8-24, Richland, WA 99354, USA

Graphical Abstract
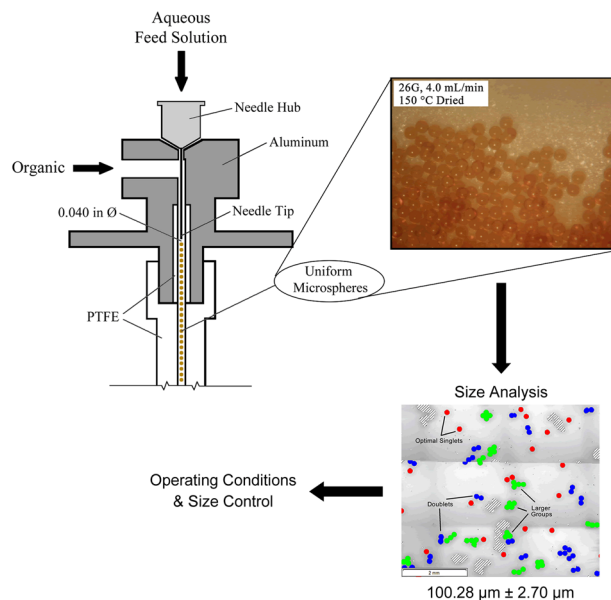
Highlights

- Microspheres with an average diameter of $100.28 \pm 2.7\ \mu m$ were produced.
- Changing flow rates yielded sphere diameters from 65–159 μm with a single orifice.
- Microspheres had excellent sphericity with measured shape factors above 0.9.
- A two-fluid nozzle sphere former was operated in the simple dripping flow regime.

1 Introduction

The internal-gelation sol–gel method provides a means to produce metal oxides from aqueous precursor solutions containing a metal nitrate, urea, and hexamethylenetetramine (HMTA). This process involves the use of HMTA to promote gelation and urea as a complexing agent. A nitrate solution containing the metal of interest is chilled separately from a concentrated solution containing HMTA and urea. Once both solutions are chilled to $0\ ^{\circ}C$, they are mixed and urea complexes the metal ion, preventing hydrolysis which would normally occur at the pH of the mixed solution [1–3]. Upon heating the mixed solution above approximately $5\ ^{\circ}C$, urea decomplexes the metal ion, allowing for a hydrolysis reaction that is driven to completion through the protonation and decomposition of HMTA, which maintains an elevated pH [1, 3–5]. Thus, the gelation process is a temperature-induced, pH-driven reaction. Through condensation of metal hydroxides and washing with dilute ammonium hydroxide, hydrated metal oxides form that are converted into pure metal oxides by heat treatments [2, 3, 6]. Therefore, sol–gel methods may be used in combination with temperature-controlled, sphere-

forming hardware to produce metal oxide microspheres. While metal oxide microspheres have potential applications in fields such as catalysts, advanced nuclear reactor fuels, nuclear thermal rocket fuels, irradiation targets, and calibration standards, the present work was motivated by an interest in the radioisotope power community to investigate low-dust-processing methods for creating plutonium-238 (^{238}Pu) heat and power sources such as those employed on NASA deep-space missions [7]. Cerium was used as a chemical and thermophysical surrogate for plutonium in this study.

Internal-gelation sol–gel techniques are being investigated as an alternative, low-dust method for fabricating granules to be pressed into plutonium-238 oxide heat source pellets [8, 9]. Heat from the alpha decay of ^{238}Pu is converted into electricity in radioisotope thermoelectric generators (RTGs) used in challenging environments such as on space vehicles used to explore the solar system. An undesirable feature of historic ^{238}Pu oxide pellet-production methods is the use of submicron, ball-milled powders. Fine particles produced by ball milling are highly dispersible due to static electricity and air currents, have very long settling times, and do not appear to agglomerate during ball-milling

[7, 10–13]. This is especially problematic since ^{238}Pu oxide is very corrosive, having its own source of heat and oxygen. Further, in the event of a breach in containment, ^{238}Pu oxide is a severe inhalation hazard [14, 15]. Particles under 10 μm in diameter tend to lodge in the lungs rather than in nasal passages [7] and cannot be completely removed, even with chelation therapy [16]. Therefore, adoption of aqueous-based microsphere-fabrication techniques to produce particles suitable for pressing into pellets is desirable to prevent powder contamination. Internal-gelation processes were recently developed for ^{238}Pu at the Pacific Northwest National Laboratory; the work presented in this article helped answer one of the preliminary questions affecting the suitability of sol–gel for this application, namely, whether microsphere "granules" can be produced in the desired size range.

Based on previously published work on ^{238}Pu oxide pellet fabrication from powder-based granules, microspheres with diameters of 100–125 μm are expected to be the best substitution. Previous studies revealed that the use of granule sizes less than 125 μm, rather than more broadly sized particles under 297 μm, resulted in a more uniform porosity and better granule-to-granule contact, which was desirable to stabilize the pellet microstructure and prevent additional shrinkage at high operating temperatures [17]. The use of microspheres with diameters near 100 μm is expected to allow thermal treatments and hot pressing such that pellets have a uniform, coarse porosity without having to process fine particulates generated during traditional powder granulation. Further, while powder-based granulates have porous, friable surfaces that generate fine

powders, microspheres minimize the surface area and have smooth surfaces. Nonuniform ^{238}Pu powder granules have resulted in the formation of dense aggregates due to self-heating during storage that adversely affected the homogeneity of pellets [18]. Therefore, the uniform size and shape of sol–gel microspheres is desirable to produce homogeneous structures as well as reduce dust generation.

Significant sol–gel development programs took place in the 1960s and 1970s in the United States using a sol-dehydration method to produce thorium, uranium, and plutonium microsphere fuels for fast-breeder reactors [19]. Sphere formation was accomplished by dispersing droplets of an aqueous suspension of particles, or sol, into an up-flowing column of 2-ethyl-1-hexanol [19–29]. The aqueous sol contained small crystallites that coalesced into a sphere upon dehydration in the organic forming fluid. As water was extracted, spheres settled out of the up-flowing column for collection, drying, and calcining. Microspheres composed of cerium surrogates as well as ^{238}Pu were made by this method with test programs, producing a broad particle-size distribution of 50–250 μm [28–30]. While modern sol–gel nuclear fuels are fabricated by internal-gelation methods, much of the droplet-forming mechanisms still used today were assessed during work with the dehydration sol–gel process.

Monodisperse microspheres can be formed using two-fluid nozzles, vibratory systems, and free-fall dripping, as depicted in Fig. 1. While free-fall dripping of spheres from multiple orifices allows for high throughput, the resulting droplet sizes are larger than those desired for most fuel applications [22]. When uniform spheres in the general
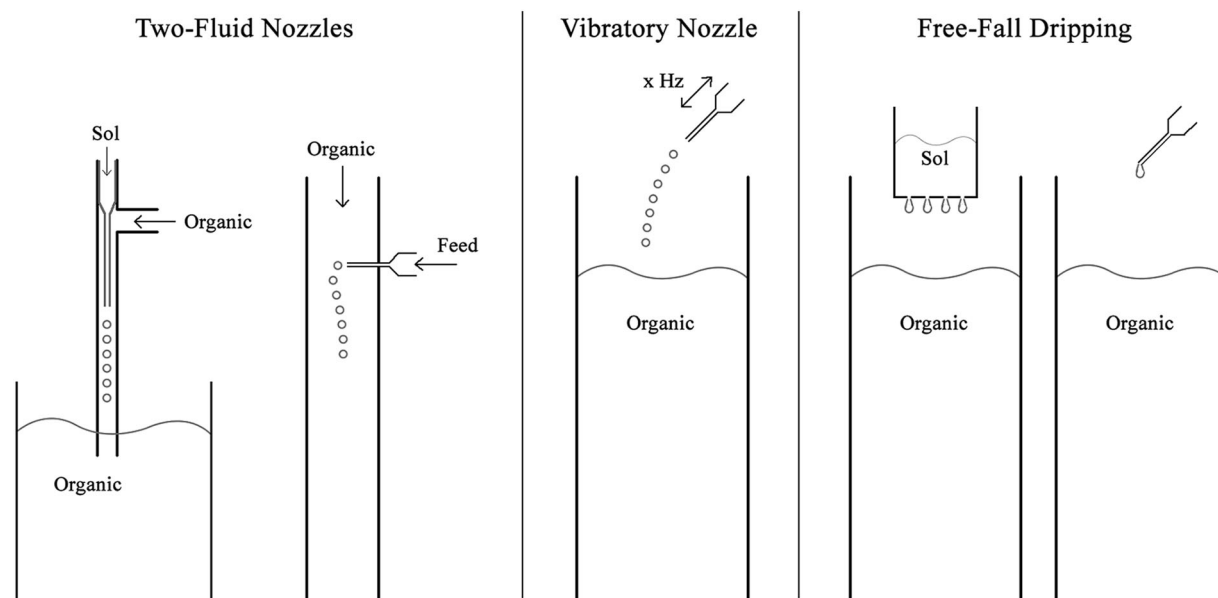

Fig. 1 Sectional views of two-fluid nozzles (left), vibratory nozzles (center), and free-fall dripping (right) techniques for droplet generation [19, 22]

range of 200–800 μm are desired, two-fluid nozzles or vibratory nozzles are typically used. Two-fluid nozzles have been operated at flow rates such that a jet of feed undergoes varicose breakup into droplets in a concurrent flow of an immiscible organic fluid [19, 22, 23]. Using two-fluid nozzles, thorium and uranium spheres were produced by sol dehydration at a variety of diameters from 88 to 590 μm with typical standard deviations of approximately 10–30% [19, 20]. [239]Pu spheres have been produced with sizes ranging from 50 to 250, 250 to 600, and 250 to 400 μm [19, 22, 30]. Similarly, [238]Pu spheres were made with diameters ranging from 50 to 250, 88 to 250, and 50 to 400 μm [20, 29, 31]. Since spheres are made one at a time, throughputs are significantly reduced as the desired sphere diameter is decreased. Therefore, production of spheres with diameters less than 300 μm was often accomplished by rapid stirring emulsification methods that yielded large batches of small spheres with a broad size distribution [2, 20, 21, 28].

Previous studies improved the monodispersity of microspheres made with two-fluid nozzles at high sol flow rates using an apparatus with a variable-frequency vibrating plunger located above the sol capillary, as shown in Fig. 2 [32–34]. Imparting a vibration on the sol near the natural sphere-formation rate resulted in improved monodispersity. The vibrating plunger, two-fluid nozzle resulted in standard deviations less than 2% for spheres with average diameters as small as 283 μm and 19% for spheres with an average diameter of 207 μm. Although spheres with diameters as small as 200 μm were produced, emphasis was placed on spheres in the 350–500-μm range [33, 34]. Similar vibrating

dispersion devices with multiple orifices were also developed to increase throughput, but resulted in poorer size uniformity and yields due to unequal divisions of sol between capillaries [33]. Since most studies were aimed at multikilogram quantities for reactor applications, sphere-production rates using two-fluid nozzles were considered too slow [19], and most work, including current TRISO fuel kernel production, focused on higher throughputs using vibratory nozzles with sphere breakup in air above the forming column [35, 36].

In the United States, vibratory nozzles are used to produce internal-gelation microspheres with final diameters of 350, 425, and 500 μm for TRISO fuels developed for high-temperature, gas-cooled reactors [35–37]. Production campaigns at Oak Ridge and scaled-up internal-gelation operations at Babcock and Wilcox for fabrication of TRISO kernels impart a vibration to the dispensing needle to cause regular breakup of feed jets. Controlled vibrations near the natural frequency of breakup also improve throughput, allowing higher flow rates of feed solutions and in some cases multiple orifices [38]. Electromagnetic vibrators are also used in the majority of internal-gelation research studies in India for a variety of applications involving microsphere oxides of thorium, uranium, and plutonium [39–47]. Fast flow rates are used to create a jet that breaks up at regular intervals and results in sphere diameters about twice that of the jet [48]. Feed solution flow rates of 10–15 mL/min are typical for 350–500 μm spheres, while rates as high as 20–30 mL/min have been achieved for 600–800 μm spheres [35, 42, 43].

More recently, another effort at Oak Ridge produced sol–gel microspheres in the 75–150 and <75 μm-diameter range [49]. Uranium oxide microspheres with diameters between 75 and 150 μm are desirable for nuclear thermal rocket tungsten cermet fuel. To achieve these small diameters with fairly high throughput, static mixers were used to generate turbulent flow and smaller droplet sizes. The use of static mixers resulted in a relatively wide distribution of particle diameters in the 75–150 μm range, as well as particles <75 μm in diameter based on variations in feed-phase and continuous-phase flow rates.

To determine whether microspheres with excellent size uniformity could be fabricated with sintered diameters near 100 μm, a sol–gel apparatus was designed and built to accommodate the production of small microspheres in the present study [8, 9]. The ability to control particle size as well as uniformity can offer advantages in fluidized-bed coating operations, as well as certain applications, such as those requiring uniformly distributed nuclear fuels, homogeneous structures, or higher densities of packed spheres with specific size ratios. Microsphere droplets were formed one at a time in a two-fluid nozzle for maximum uniformity using a configuration allowing for different sized needles to
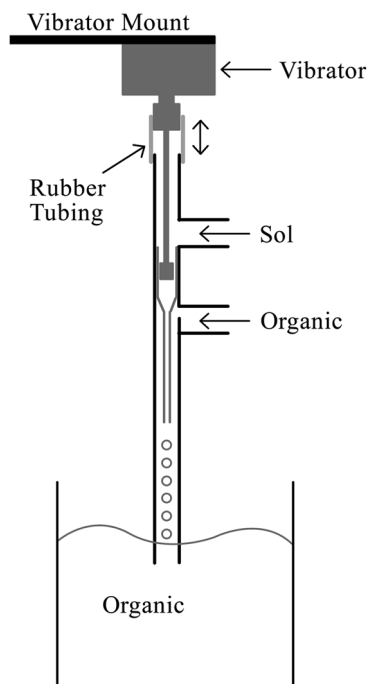

Fig. 2 Sectional view of a vibratory two-fluid nozzle [32, 33]

be used interchangeably. The flow rate of silicone oil flowing past the needle (stripping oil) in the sphere-forming device could also be adjusted easily during a production run. Separate batches of microspheres were prepared using different combinations of needle size and stripping oil flow rate to determine the effect on particle size and monodispersity.

2 Experimental

2.1 Materials

Reagents used to fabricate cerium oxide microspheres included Acros Organics ceric ammonium nitrate (CAN) with 99.5% purity (lot #A0331425), Sigma-Aldrich HMTA with 99.5% purity (lot #SZBA2210V), Sigma-Aldrich urea with 99.5% purity (lot #BCBD7141V), and Sigma-Aldrich 28% ammonium hydroxide (batch #MKBG2814). Reagent-grade trichloroethylene (TCE) and isopropyl alcohol (IPA) were used for washing microspheres. Deionized water from a RiOs-DI 3 UV Millipore system was used for solution preparation and microsphere washing. An acid-deficient CAN solution was prepared by dropwise addition of concentrated ammonium hydroxide (NH_4OH) to achieve an OH^-/Ce^{4+} ratio of 0.75. The CAN solution was mixed with a 3.18 M solution containing HMTA and urea with an $HMTA/Ce^{4+}$ ratio of 2.0.

2.2 Apparatus and gelation conditions

A custom sol–gel apparatus was designed and constructed for microsphere production. Gas pressure was applied to the mixed-feed vessel and stripping-oil vessel for pneumatic flow. Mixed feed solution was metered through a hypodermic needle into a co-flowing stream of chilled stripping oil in a sphere-forming device, as shown in Fig. 3. In this device, the needle tip was positioned inside a 1-mm-diameter PTFE channel where droplets were sheared off from the needle tip by laminar, co-flowing stripping oil. The outlet of the sphere-forming device deposited microspheres into a much larger laminar flow of hot silicone oil falling down the inner region of a jacketed column under the influence of gravity. Microspheres were heated and gelled while flowing down the inner region of the jacketed column and were collected in a mesh sieve at the column outlet. Silicone oil flowing down the inner region of the jacketed column was recirculated using a peristaltic pump and preheated in a heat-tape-wrapped vessel prior to entering the column. This silicone oil, which heated spheres and caused them to gel, was maintained at approximately 80 °C. A Julabo F25 heating circulator was used to maintain separate oil at approximately 130 °C and pump it up through the outer region of a jacketed column in order to heat the oil stream flowing down through the inner region. A Julabo FL601 recirculating chiller was used to chill feed solutions, stripping oil, the sphere-forming device, and transfer lines from the mixed-feed vessel to the sphere-forming device. The major components of the sol–gel apparatus are shown in Fig. 4.

Prior to sizing experiments, a flow meter measuring the rate of stripping oil flow past the dispensing needle was calibrated over the range of 0.5–8 mL/min using a stopwatch and graduated cylinders to generate a flow vs. voltage curve at the equilibrium stripping-oil temperature of approximately 5 °C. New stainless-steel needles from the Hamilton Company were cleaned using fresh aqua regia and deionized water and dried before use. At the end of the experiments, feed-transfer lines were washed with dilute nitric acid and deionized water to prevent the solidification of the remaining feed solutions that could cause clogging after the system returned to room temperature.

Nine batches of spheres were collected using three needle sizes and three stripping oil flow rates. Needles with inner diameters of 260 μm (26 G), 184 μm (28 G), and 108 μm (32 G) were used. For each needle size, spheres were collected in separate mesh baskets at each stripping oil flow rate of approximately 1.5, 4.0, and 6.5 mL/min. Stripping oil flow rates were varied from slow to intermediate to fast, corresponding to maximum, medium, and minimum sphere sizes, respectively. Change in the feed flow rate between samples was kept to a minimum and was calculated to be approximately 0.15 mL/min. Once microsphere production began and the desired stripping-oil speed was set, an overpressure of 3–4.5 psi was applied to the feed solution in order to adjust the rate of sphere formation such that inter-sphere spacing in the gelation column was minimal. With
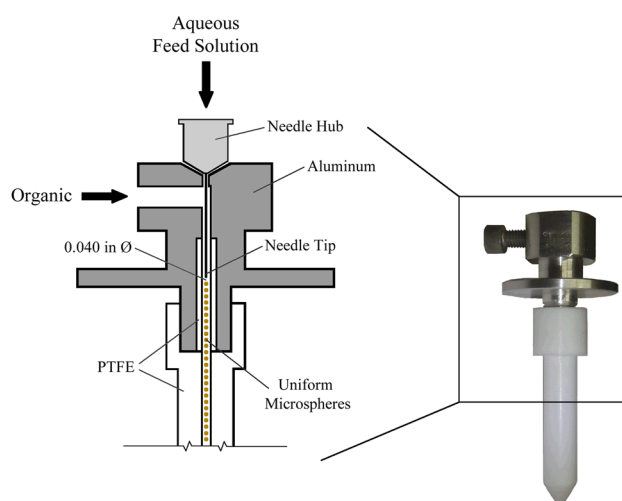

Fig. 3 Sectional view (left) and image (right) of the sphere-forming device depicting uniform microspheres being stripped from a dispensing needle in co-flowing silicone oil in a two-fluid nozzle arrangement

the desired parameters established, spheres were collected in one of several small, mesh baskets to allow for separate recovery and analysis of samples. When a sufficient quantity was produced, the mesh basket was removed from the system to a bath of silicone oil on a hot plate set to 85 °C to cure for 20 min. This procedure was repeated for the remaining stripping-oil speeds and again for each needle. Silicone oil was periodically degassed in the circulation loop to prevent the formation of bubbles in the gelation column, which otherwise interacted with ungelled microspheres and caused coalescence.

After cooling overnight, each mesh basket containing a unique sample was fit into its own 50-mL centrifuge tube for washing to remove silicone oil and impurities. Most silicone oil was removed by two, 15-min washes with TCE.

Next, residual silicone oil was removed during two, 15-min washes with 50% TCE and 50% IPA. Spheres were then washed with two, 20-min washes with 50% IPA and 50% 0.5 M NH$_4$OH followed by three, 30-min washes with 0.5 M NH$_4$OH. In each case, wash volumes were 30 mL. Effluents from 0.5 M NH$_4$OH washes were monitored for conductivity using a ThermoScientific Orion Star A215 pH/ conductivity meter calibrated at 1.413 and 12.9 mS/cm to ensure that effluent conductivities were reduced to values similar to that of the stock 0.5 M NH$_4$OH used for washing. Spheres were then rinsed with deionized water, placed in a large beaker of deionized water heated to 85 °C for 2 h, and allowed to cool. After reaching room temperature, spheres were rinsed with deionized water and transferred to alumina boats to air-dry using 75% IPA and 25% deionized water.
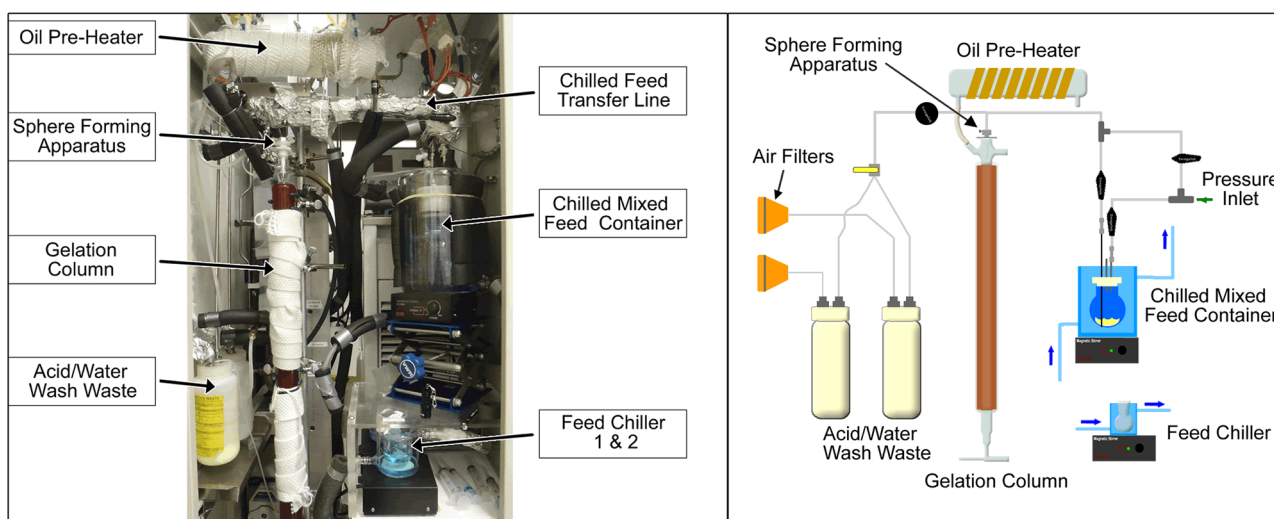

Fig. 4 Image (left) and schematic (right) of the major components of the sol–gel apparatus used for microsphere production
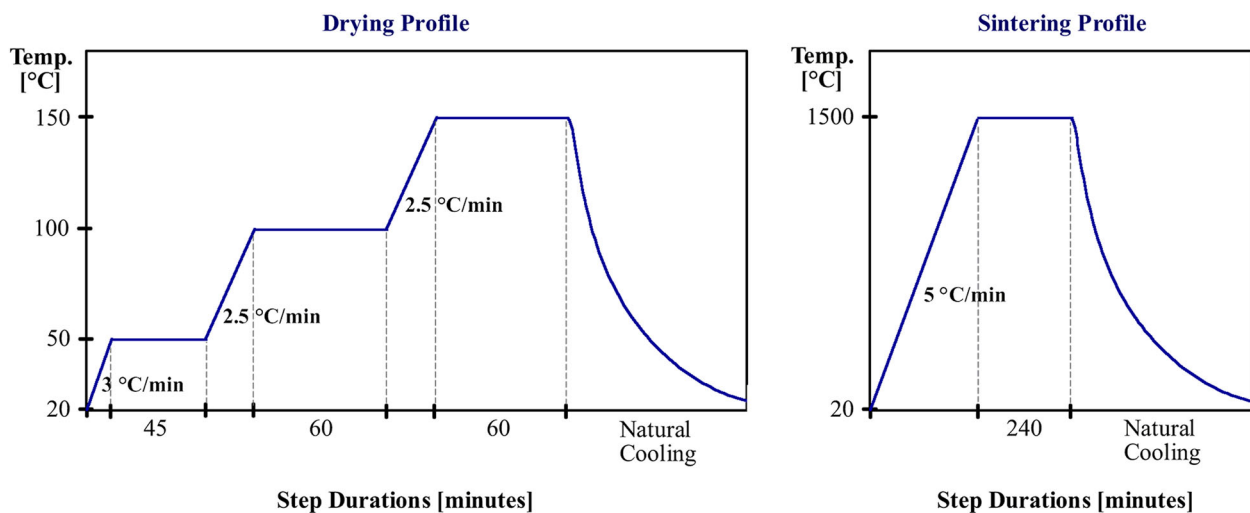

Fig. 5 Heat-treatment profiles for microspheres drying in a low-temperature furnace prior to sintering in a high-temperature furnace

After air-drying at ambient temperature for several days, spheres were heated to 150 °C, according to the drying profile in Fig. 5, to allow slow evolution of the remaining volatiles to avoid cracking. After dwelling at 150 °C for 1 h, spheres were cooled to room temperature and transferred to a high-temperature box furnace for sintering at 1500 °C with a ramp rate of 5 °C/min, as shown in the sintering profile in Fig. 5.

2.3 Size and shape analysis

After sintering, spheres were dispersed on glass slides for imaging using an optical microscope. Photoresist was applied to the glass slides prior to loading with microspheres to act as an adhesive, preventing spheres from rolling off the slide and contaminating the microscope and clean-room facilities. Microspheres were imaged using bright-field microscopy with 5–10× magnification using an Olympus BX-51 fluorescence microscope. A motorized stage and software allowed for automated imaging of a large area by stitching many images into a single photograph of the entire slide. One slide was prepared for each of the sizing conditions, allowing size analysis of hundreds of spheres in each case. Olympus Stream micro-imaging software allowed for post processing of images to measure the mean radius and shape factor of particles. The degree to which particles represented a perfect sphere was measured using a shape factor, defined as:

$$\text{Shape factor} = 4\pi \frac{\text{Area}}{\text{Perimeter}^2}, \tag{1}$$

which has a value of 1 for a perfect circle.

Average sphere diameters were determined using a multistep process with the sizing software. First, the program was run with broad size constraints to include all particles sized in the analysis. This initial scan was used to generate a histogram of mean radius, which was segregated into color-coded regions corresponding to custom-size bins. Particles in each size bin then appeared in the image with their corresponding color for visual discrimination of particle categories. Based on the color-coded results, a second analysis was run to consider both size and shape. Shape factors were obtained for particles in the desired size window, and a mean radius vs. shape-factor distribution plot was used to define a two-dimensional region of interest. As will be discussed in the next section, consideration of both parameters allowed for the most accurate determination of sphere-size distribution by eliminating mis-imaged particles, overlapping microspheres, and shadows that distorted contrast-based measurements. Due to the difficulties with the optical approach, the shape factor and particle diameters were also measured for another sample, produced by the same equipment and approach, using ImageJ software and a

scanning-electron microscope (SEM) image. In this case, microspheres were sieved and distributed on double-sided copper tape on the SEM sample stub to avoid overlapping and shadows.

3 Results/discussion

3.1 Process improvements

Initially, coalescence of ungelled microspheres was an impediment to creating monodisperse particles. Although uniform spheres were formed using the two-fluid nozzle, coalescence in the gelation column created large spheres prior to gelation. Coalescence was prevalent when oil in the inner region of the jacketed column was stagnant, which caused crowding of spheres injected from the sphere-forming device. This effect was mitigated by introducing a recirculating, laminar flow of silicone oil through the inner region of the jacketed column to sweep the spheres through the column after injection from the sphere-forming device. Nucleation, growth, and travel of gas bubbles also occurred in the inner region of the jacketed column. Bubbles traveling in the column disrupted microsphere flow and also caused coalescence. Bubble generation was mitigated by occasional degassing of circulating silicone oil in an ultrasonic bath. Coalescence was mitigated prior to producing microspheres for sizing experiments.

3.2 Size analysis

Microspheres produced using different needle sizes and stripping oil flow rates had measured diameters ranging from 65 to 211 μm with standard deviations in most cases less than 4%. Average diameters and standard deviations for samples are summarized in Table 1. Constraints imparted on particle size and shape factor in the analysis software are also provided in Table 1. Needle size appeared to have a more significant impact on diameter as the stripping-oil speed was reduced. The diameter of microspheres produced at the fastest stripping-oil speeds varied by less than 10% across needles compared to 22–25% for intermediate and slower oil speeds. The range of microsphere sizes possible increased with larger needles; microspheres produced by the 26-gauge needle encompassed nearly the entire size range of all needles tested.

While analyzing sphere sizes, it became apparent that the software was unable to accurately determine the diameter of microspheres in contact with one another and would assign an oversized, collective diameter. Therefore, size-threshold constraints were employed to eliminate from statistical analysis groupings of two or more microspheres that the software could not discriminate and measure them correctly.

Table 1 Constraints applied to optical image processing and the resulting microsphere sizes as a function of needle gauge and stripping oil flow rate

	26-Gauge needle			28-Gauge needle			32-Gauge needle		
	1.5 mL/min	4 mL/min	6.5 mL/min	1.5 mL/min	4 mL/min	6.5 mL/min	1.5 mL/min	4 mL/min	6.5 mL/min
Input constraints									
Mean diameter range [μm]	194–238	100–160	50–90	150–220	90–110	58–88	144–180	84–120	54–78
Shape-factor range	0.82–1	0.9–1	0.93–1	0.82–1	0.88–1	0.87–1	0.8–1	0.86–1	0.92–1
Results									
Average diameter [μm]	211.28	127.9	70.56	176.34	100.28	71.85	159.05	99.21	65.5
Standard deviation [μm]	4.71	7.40	5.48	5.39	2.70	3.92	4.92	3.77	2.43
Standard deviation [%]	2.23	5.78	7.77	3.06	2.69	5.46	3.09	3.80	3.71
Spheres counted	560	446	247	247	492	809	972	1395	2113

Analysis indicates that microspheres in the 65–211-μm diameter range were produced with excellent size uniformity
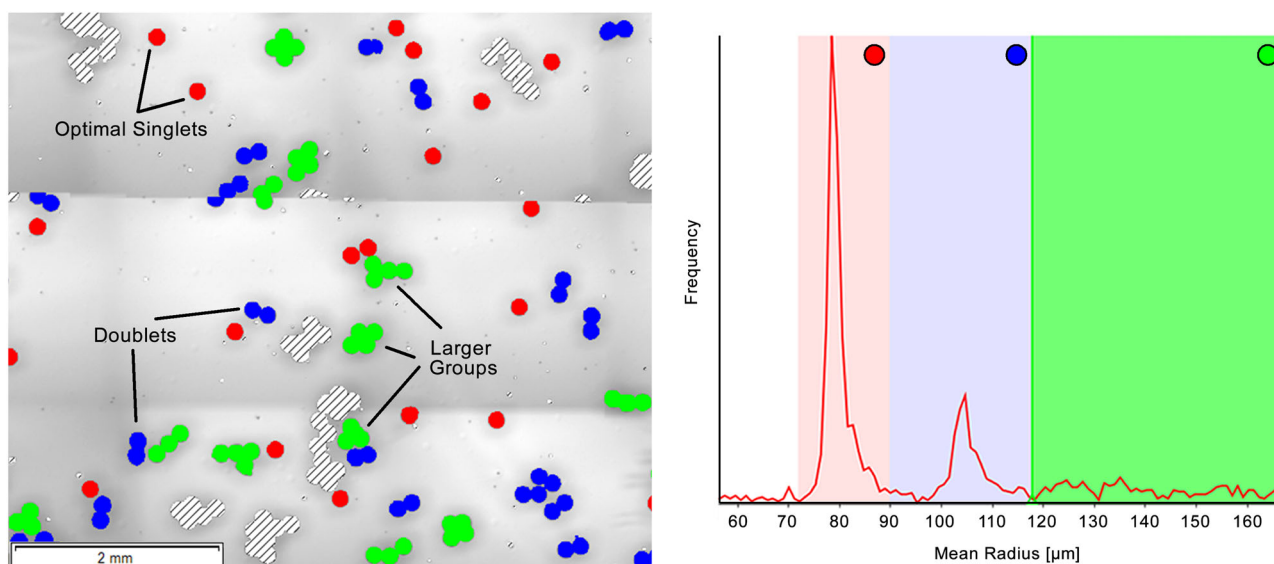

Fig. 6 Image processed by Olympus Stream to identify size regimes (left) and plot of particle-size frequency (right) indicating that sizes were grouped into categories of single spheres, touching spheres (doublets), and larger groups of spheres

In each image analyzed, unique thresholds were selected to ensure that individual microspheres with diameters smaller or larger than the mean were not discarded from analysis. Upon scanning images for particle sizes, it became apparent that the software identified multiple size modes, as indicated in Fig. 6. Individual microspheres comprised the major group and are shown in red. Another group was identified corresponding to two adjacent spheres, or doublets. Additionally, larger sizes recorded by the software were easily identified as collections of three or more microspheres. Based on this analysis, size windows were defined as constraints for average microsphere-diameter analysis while excluding collections of two or more spheres. Lower bounds were also set to eliminate dust and microspheres cut into half by image-stitching operations from analysis.

3.3 Shape analysis

As indicated in Table 1, shape factors of 0.8–1.0 were applied as constraints in addition to size windows. The shape-factor constraint allowed for improved discrimination of single particles from collections of particles and excluded particles with photoresist shadows from analysis, improving the measurement of actual microsphere diameters. As can be seen in Fig. 7, ripples in the photoresist around some spheres resulted in shadows that the software could not differentiate from the sphere, causing it to misrepresent the actual microsphere size and shape. However, not all single microspheres had shadows and misinterpreted microspheres were removed from analysis by application of a shape-factor constraint. Shape-factor windows were as wide as
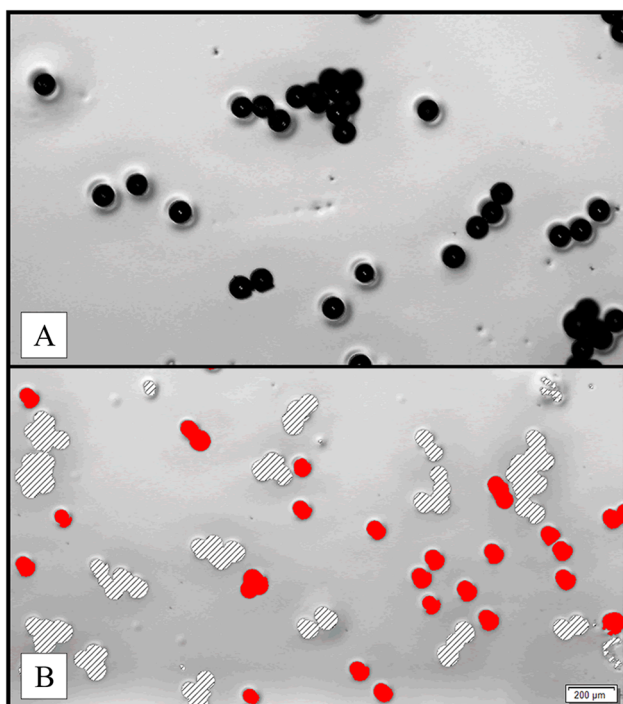
Fig. 7 Image processed by Olympus Stream to calculate shape factor, unprocessed (**a**) and processed (**b**), showing that dimples in the photoresist caused an inaccurate representation of diameters and shape for some spheres that had to be removed from analysis

Fig. 8 SEM image of CeO_2 microspheres with those analyzed by ImageJ highlighted and numbered

0.8–1.0 and as restrictive as 0.93–1.0. The exclusion of microspheres based on shape factor was not expected to unreasonably improve the standard deviation of average microsphere diameters based on observations and the constraint windows selected.

To obtain an accurate measurement and verify that constraints applied for sizing analysis were reasonable, the shape factor was also measured explicitly. Olympus Stream micro-imaging software was used to analyze images of spheres that did not have photoresist shadows, yielding shape factors of 0.95–1.0. Additionally, spheres from another sample, produced by the same equipment and approach, were imaged on an SEM and processed using ImageJ software to confirm the typical shape factor and particle uniformity. This approach was preferable for measurements, but had limits on the number of spheres that could be assessed compared to the optical methods. Over 80 nonoverlapping, integral spheres were analyzed and are highlighted and numbered in Fig. 8. ImageJ analysis of the SEM image yielded shape factors ranging from 0.900 to 0.926 with an average shape factor of 0.912 ± 0.0057 and an average diameter of 115 ± 6.3 μm.

3.4 Impact of needle size and flow rates

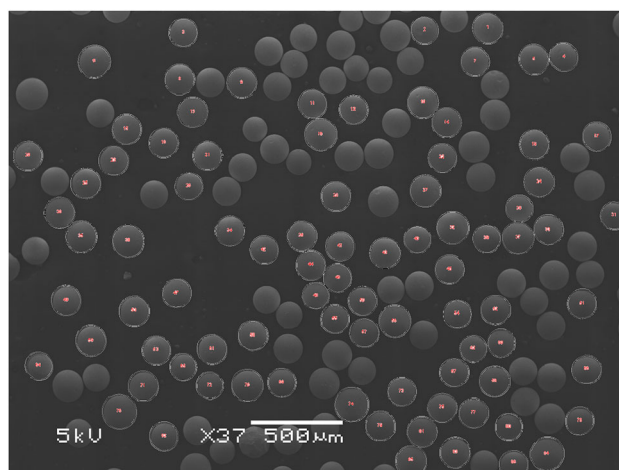While the average microsphere diameter was observed to shrink as needle diameter decreased, the most significant parameter controlling microsphere size was the stripping-oil speed, as shown in Fig. 9. While microspheres produced using the 26-gauge needle at a stripping oil flow rate of 1.5 mL/min were the largest produced in the experiment with an average diameter of 211 μm, increasing the stripping oil flow rate to 6.5 mL/min resulted in microspheres with an average diameter of 70.5 μm, which was within 5 μm of the smallest spheres produced using the smallest needle, as shown in Fig. 9b. Microspheres produced using a 26-gauge needle are shown in Fig. 10 after drying at 150 °C and after sintering to 1500 °C for 4 h. Pale-yellow, translucent microspheres in the air-dried state became translucent orange after drying at 150 °C and an off-white, pearl color after sintering.

The degree of monodispersity observed in microspheres suggests that droplet formation occurred in a simple-dripping flow regime where spheres of a uniform size were stripped from the dispensing needle at regular intervals. Microfluidics experiments producing uniform emulsions of water or solvents in oil have documented the production of 2–200 μm particles with minimum standard deviations less than 3% [50]. These experiments made use of similar sphere-stripping techniques in the dripping flow regime to achieve highly uniform particles. Therefore, the narrow size distributions of 2.23–3.80% standard deviation reported in Table 1 for cerium oxide microspheres produced in this work were comparable to those observed in similar microfluidics equipment in the literature. Incidences of higher standard deviations in three test cases from 5.46 to 7.77% are believed to be elevated in part due to misinterpretation of shadows and particle overlap by optical image-analysis software.

Droplet size is dependent on the flow rates, densities, and viscosities of the continuous and dispersed liquids in the sphere-forming device, as well as the needle diameter and
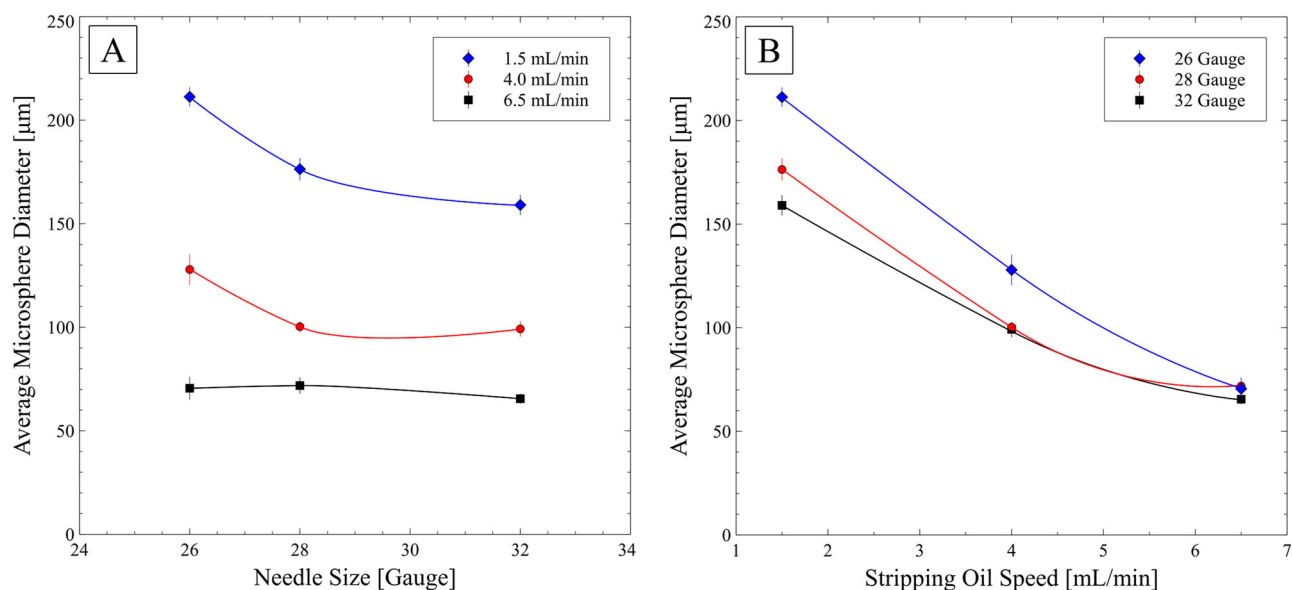
Fig. 9 Plotting microsphere diameter as a function of needle size (**a**) and as a function of stripping-oil speed (**b**) indicates that stripping oil flow rates had a more significant impact on microsphere diameter than the size of the dispensing needle

channel diameter. In this work, the dispersed feed solution had a flow rate of approximately 0.15 mL/min through needles with inner diameters from 108 to 260 μm, while the continuous oil stream had a flow rate of 1.5–6.5 mL/min in a PTFE channel with an inner diameter of 1 mm. Silicone oil with a room-temperature kinematic viscosity of 100 cSt, density of 960 kg/m³, and surface tension of approximately 0.02 N/m was used. A reported value of 0.025 N/m for interfacial tension between silicone oil and water was assumed for the interfacial tension between the aqueous feed solution and silicone oil [51]. These parameters allowed for the calculation of Weber (We), capillary (Ca), and Reynolds (Re) numbers according to the following equations:

$$We = \frac{\rho v^2 l}{\sigma}, \qquad (2)$$

$$Ca = \frac{\mu v}{\sigma}, \qquad (3)$$

$$Re = \frac{\rho v D_H}{\mu}, \qquad (4)$$

where ρ is the density, v is the velocity, l is the characteristic length, σ is the surface or interfacial tension, μ is the dynamic viscosity, and D_H is the hydraulic diameter. The calculated values for the equipment and flow rates used in this study were We = 0.007, Ca = 0.1–0.8, and Re = 1.

The simple-dripping flow regime for droplet formation is characterized by slow flow rates, whereby liquid accumulates in a droplet until the force from gravity exceeds the cohesive forces in the liquid, and a droplet breaks off from

an orifice at a distance of approximately one droplet diameter. During sol–gel microsphere formation, the force of gravity can be ignored in the dispersion apparatus, but it is replaced with shear forces from the coaxial flow of silicone oil. At slow feed solution flow rates, droplets grow on the tip of the needle until shear forces exceed cohesive forces in the feed, and the droplet is stripped off into the oil flow [52]. As long as flow rates remain constant, droplet formation occurs at a set frequency. This simple dripping behavior transitions to complex dripping at faster flow rates and is characterized by quasi-periodic or chaotic sphere sizes [53–55]. At still faster flow rates of feed solutions, liquid jets are formed. The jetting regime is characterized by Rayleigh breakup of liquid jets. At these faster flow rates, a thin column of fluid forms due to inertia and the influence of gravity. Deformations in this jet column, caused by varicose perturbations, result in regions of increased and decreased diameter [48, 52]. Variations in the jet diameter result in regions of high and low pressure, which cause further pinching of the jet into droplets due to surface tension. Jet breakup into spheres occurs to minimize surface area. In a two-fluid nozzle with silicone oil flowing past the dispensing needle, gravity is again ignored and the column of feed, or jet, is produced by the inertial energy of the feed and shear forces from the faster-flowing silicone oil.

While many previous sol–gel systems have produced uniform microspheres larger than 200–300 μm using vibration to promote regular jet breakup, the work performed in this study is representative of the simple dripping regime. The relatively linear change in microsphere size while changing the stripping-oil velocity at fixed feed flow
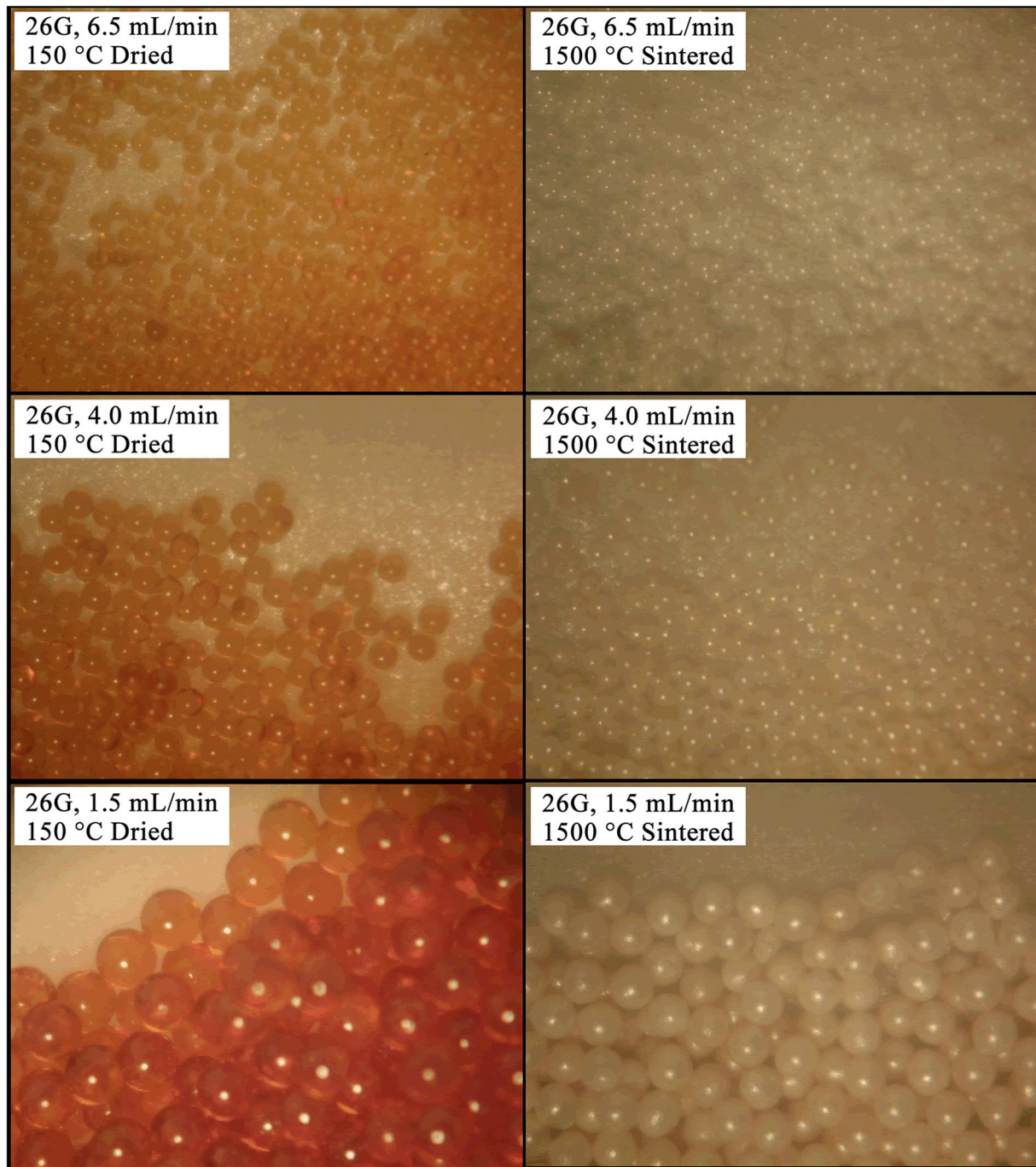
Fig. 10 Dried (left) and sintered (right) microspheres produced using a 26-gauge needle as a function of stripping oil flow rates

rates observed in Fig. 9b is indicative of droplet formation in the simple dripping mode [56]. Additionally, increasing the feed flow rate at a fixed stripping-oil velocity caused the eventual formation of irregular-sized microspheres one would expect from complex dripping or uncontrolled jetting [53–55]. Although many different methods are used to predict the transition from dripping to jetting, it can be estimated to occur when the sum of the Weber and capillary number is approximately equal to 1 [52]. Alternatively, uniform droplet formation at a fixed frequency can be assumed if We ≪ 1 [53]. The Weber number of 0.007, capillary numbers of 0.1–0.8, and uniform microspheres representative of this work correspond to simple periodic dripping according to both of these general rules. However,

while operating with faster stripping-oil speeds and higher feed-solution overpressures than those discussed in this study, the sol–gel apparatus has also transitioned to complex dripping or jetting regimes characterized by wider particle-size distributions and fast droplet-production rates.

While using flow rates that resulted in uniform microspheres, particle sizes were controlled primarily by varying the stripping oil flow rate rather than changing the overpressure on feed solutions. Observation of microspheres produced at a variety of stripping-oil speeds and feed-solution overpressures revealed that desirable stripping-oil speeds encompassed a wide range of flow rates, spanning nearly an order of magnitude from 1 to 9 mL/min. However, desirable feed-solution overpressures were in a much smaller range from 3 to 4.5 psi. Within the range of 3–4.5 psi, the change in microsphere size was negligible compared to the change in microsphere size with variation of the stripping-oil speed. For this reason, the stripping-oil speed was used to vary microsphere size, while the feed overpressure was used to adjust the frequency of microsphere formation. However, if the feed flow rate crossed a threshold value, generally above 4.5 psi, uniform microspheres in a single-file line transitioned into a distributed stream of larger, polydisperse spheres. As discussed, these observations led to the belief that optimal flow conditions for monodisperse microsphere formation existed in the dripping regime where droplet formation occurred due to shearing forces from stripping oil rather than those in the jetting regime.

Analysis of microsphere sizes produced using different needle gauges and stripping oil flow rate revealed that 26-gauge needles had the greatest utility of those tested. While varying the stripping oil flow rate decreased the microsphere diameter by as much as a factor of 3, reduction in microsphere diameters with smaller needles was only 7.7–33%. The range of sizes from the 26-gauge needle encompassed 96.5% of the entire range of spheres produced with all three needles. Therefore, while small needles can be used to make uniform microspheres of the desired size, using larger needles and higher stripping oil flow rates is desirable to minimize the likelihood of needle clogging.

The observed cerium oxide microsphere-size distributions are expected to be suitable for ^{238}Pu oxide pellet pressing as well as other fuel applications. Microsphere-based fuels using a mixture of sphere sizes could benefit from improved control over the diameter of the smallest spheres to improve packing fractions. Small microspheres may also prove to be useful for microsphere-based irradiation targets for medical isotope production. Additionally, the use of spheres of a controlled size could ease dye loading and improve homogeneity for more conventional fuel pellets produced from microspheres compared to traditional methods using angular powders.

4 Conclusions

Techniques and equipment were developed to produce microspheres with controlled diameters from 65 to 211 μm using flow conditions that resulted in simple periodic dripping for droplet formation. Excellent monodispersities for internal-gelation microspheres in this size range were achieved that are expected to be suitable for a number of applications requiring monodisperse particles, including ^{238}Pu oxide pellets. Variation in microsphere size caused by coalescence was effectively reduced by introducing laminar-flow conditions in the gelation column and by preventing bubble formation by periodic silicone oil degassing. Also, microspheres with diameters near 100 μm were produced using larger gauge needles and faster stripping oil flow rates, which is expected to result in a lower incidence of needle clogging.

Compliance with ethical standards

References

1. Brugghen FW vd, Noothout AJ, Hermans MEA et al. (1970) A U (VI)-process for microsphere production. In: Wymer RG, Lotts AL (eds) Sol-gel processes and reactor fuel cycles. Oak Ridge National Laboratory, Gatlinburg, Tennessee
2. Kanij JBW, Noothout AJ, Votocek O (1973) The KEMA U(VI)-process for the production of UO_2 microspheres. In: Hermans MEA (ed) Proceedings of a panel on sol-gel process for fuel fabrication. International Atomic Energy Agency, Vienna
3. Collins JL, Lloyd MH, Fellows RL (1987) The basic chemistry involved in the internal-gelation method of precipitating uranium as determined by pH measurements. Radiochim Acta 42:121–134
4. Collins JL, Lloyd MH, Fellows RL (1984) Effects of process variables on reaction mechanisms responsible for ADUN hydrolysis, precipitation, and gelation in the internal gelation gel-sphere process. Oak Ridge National Laboratory, Oak Ridge, Tennessee

5. King CM, King RB, Garber RA et al. (1990) Magnetic resonance as a structural probe of a uranium (VI) sol-gel process. MRS Online Proceedings Library, San Francisco, CA

6. Cordfunke EHP (1972) The system $UO_2(NO_3)_2$-UO_3-H_2O. J Inorg Nucl Chem 34:531–534

7. Borland M, Frank S, Lessing P et al. (2008) Evaluation of aqueous and powder processing techniques for production of Pu-238 fueled general purpose heat sources. Idaho National Laboratory, Idaho Falls, Idaho

8. Katalenich JA (2014) Production of monodisperse, crack-free cerium oxide microspheres by internal gelation sol-gel methods. University of Michigan, Ann Arbor, Michigan

9. Katalenich JA (2017) Production of cerium dioxide microspheres by an internal gelation sol–gel method. J Sol Gel Sci Technol 1–10. https://doi.org/10.1007/s10971-017-4345-8

10. Kent RA (1979) LASL fabrication flowsheet for GPHS fuel pellets. Los Alamos Scientific Laboratory, Los Alamos, New Mexico

11. Duncan A, Kane M (2009) Properties and behavior of Pu-238 relevant to decontamination of building 235-F. Savannah River Nuclear Solutions, Aiken, South Carolina

12. Congdon JW (1996) Physical behavior of Pu-238 oxide. Westinghouse Savannah River Company, Aiken, South Carolina

13. Icenhour AS (2005) Transport of radioactive material by alpha recoil. Oak Ridge National Laboratory, Oak Ridge, Tennessee

14. Office of Oversight, Rollow T (2000) Type A accident investigation of the March 16, 2000 Plutonium-238 multiple intake event at the plutonium facility Los Alamos National Laboratory. U.S. Department of Energy, Office of Environment, Safety, and Health, Los Alamos, New Mexico

15. Department of Energy, Germantown, MD. National Nuclear Security Administration (2003) Type B accident investigation of the August 5, 2003 Plutonium-238 multiple uptake event at the plutonium facility. Los Alamos National Laboratory, New Mexico, Technical Information Center Oak Ridge Tennessee

16. Serandour AL, Tsapis N, Gervelas C et al. (2007) Decorporation of plutonium by pulmonary administration of Ca-DTPA dry powder: a study in rat after lung contamination with different plutonium forms. Radiat Prot Dosim 127:472–476. https://doi.org/10.1093/rpd/ncm300

17. Bickford DF, Rankin DT (1975) Fabrication of granule and pellet heat sources from oxalate-based [238]PuO_2. Savannah River Laboratory, Aiken, South Carolina

18. Folger RL (1980) [238]Pu fuel form processes bimonthly report—May/June 1979. Savannah River Laboratory, Aiken, South Carolina

19. Wymer RG (1968) Laboratory and engineering studies of sol-gel processes at Oak Ridge National Laboratory. Oak Ridge National Laboratory, Oak Ridge, Tennessee

20. Ferguson DE (1968) Chemical technology division annual progress report for period ending 31 May. Oak Ridge National Laboratory, Oak Ridge, Tennessee

21. Haas PA, Bond WD, Lloyd MH, McBride JP (1966) Sol-gel process development and microsphere preparation. In: Wymer RG (ed) Second international thorium fuel cycle symposium. U.S. Atomic Energy Commission, Gatlinburg, Tennessee

22. Haas PA, Haws CC, Kitts FG, Ryon AD (1967) Engineering development of sol-gel processes at the Oak Ridge National Laboratory. Oak Ridge National Laboratory, Turin, Italy

23. Wymer RG (1965) Preliminary studies of the preparation of UO_2 microspheres by a sol-gel technique. Oak Ridge National Laboratory, Oak Ridge, Tennessee

24. Haas PA (1969) Sol-gel preparation of spheres: design and operation of fluidized bed columns. Oak Ridge National Laboratory, Oak Ridge, Tennessee

25. Haas PA, Clinton SD, Kleinsteuber AT (1966) Preparation of urania and urania-zirconia microspheres by a sol-gel process. Can J Chem Eng December: 348–353

26. Dewell EH (1969) Gel-addition process chemical studies—Quarterly Progress Report No. 9. Babcock & Wilcox, Lynchburg, Virginia

27. Finney BC, Haas PA (1972) Sol-gel process—engineering-scale demonstration of the preparation of high-density UO_2 microspheres. Oak Ridge National Laboratory, Oak Ridge, Tennessee

28. Grove GR, Kelly DP, Vallee RE, Lonadier, FD, Brown WB (1967) Mound Laboratory Isotopic Power Fuels Programs: January–March, 1967. Mound Laboratory

29. Bradley JE, Grove GR, Gnagey LB, Sheidler WC, Huddleston FM, Lonadier FD, Wittenberg LJ, Kershner CJ, Kelly DP (1967) Mound Laboratory Isotopic Power Fuels Programs: October–December 1966. Mound Laboratory

30. Grove GR, Kelly DP, Vallee RE, Lonadier, FD, Brown WB (1967) Mound Laboratory Isotopic Power Fuels Programs: April–June 1967. Mound Laboratory

31. Plymale DL, Smith WH (1968) The preparation of plutonium-238 dioxide microspheres by the sol-gel process. Mound Laboratory, Miamisburg, Ohio

32. Wymer RG (1973) Sol-gel processes at Oak Ridge National Laboratory: development, demonstration, and irradiation tests. Oak Ridge National Laboratory, Oak Ridge, Tennessee

33. Haas PA, Lackey WJ (1973) Improved size uniformity of sol-gel spheres by imposing a vibration on the sol in dispersion nozzles. Oak Ridge National Laboratory, Oak Ridge, Tennessee

34. Haas PA (1975) Formation of liquid drops with uniform and controlled diameters at rates of 10^3 to 10^5 drops per minute. Am Inst Chem Eng 21:383–385

35. Collins JL (2004) Production of depleted UO_2 kernels for the advanced gas-cooled reactor program for use in TRISO coating development. Oak Ridge National Laboratory, Oak Ridge, Tennessee

36. Hunt RD, Collins JL (2004) Uranium kernel formation via internal gelation. Radiochim Acta 92:909–915. https://doi.org/10.1524/ract.92.12.909.55110

37. Barnes CM, Richardson WC, Husser D, Ebner M (2008) Fabrication process and product quality improvements in advanced gas reactor UCO kernels. In: Fourth international topical meeting on high temperature reactor technology, American Society of Mechanical Engineers, 177–188

38. Haas PA (1992) Formation of uniform liquid drops by application of vibration to laminar jets. Ind Eng Chem Res 31:959–967

39. Kumar N, Sharma RK, Ganatra VR et al. (1991) Studies of the preparation of thoria and thoria-urania microspheres using an internal gelation process. Nucl Technol 96:169–177

40. Ganatra VR, Kumar N, Suryanarayana S et al. (2008) Process and equipment development for the preparation of small size UO_2 microspheres by jet entrainment technique. J Radioanal Nucl Chem 275:515–522. https://doi.org/10.1007/s10967-007-6998-1

41. Ganguly C (1993) Sol-gel microsphere pelletization: a powder-free advanced process for fabrication of ceramic nuclear fuel pellets. Bull Mater Sci 16:509–522

42. Pai RV, Mukerjee S, Vaidya V (2004) Fabrication of (Th,U)O2 pellets containing 3 mol% of uranium by gel pelletisation technique. J Nucl Mater 325:159–168. https://doi.org/10.1016/j.jnucmat.2003.11.010

43. Sood DD (1988) Fuel chemistry division progress report for 1988. Bhabha Atomic Research Institute, Mumbai, Maharashtra, India

44. Vaidya VN, Mukherjee SK, Joshi JK et al. (1987) A study of chemical parameters of the internal gelation based sol-gel process for uranium dioxide. J Nucl Mater 148:324–331

45. Suryanarayana S, Kumar N, Bamankar YR et al. (1996) Fabrication of UO$_2$ pellets by gel pelletization technique without addition of carbon as pore former. J Nucl Mater 230:140–147

46. Pai RV, Dehadraya JV, Bhattacharya S et al. (2008) Fabrication of dense (Th,U)O$_2$ pellets through microspheres impregnation technique. J Nucl Mater 381:249–258. https://doi.org/10.1016/j.jnucmat.2008.07.044

47. Sood DD (2011) The role of sol–gel process for nuclear fuels—an overview. J Sol Gel Sci Technol 59:404–416. https://doi.org/10.1007/s10971-010-2273-y

48. Merrington AC, Richardson EG (1947) The break-up of liquid jets. Proceeedings Phys Soc 59:1–13

49. Hunt RD, Collins JL, Johnson JA, Cowell BS (2017) Production of 75–150 μm and 75 μm of cerium dioxide microspheres in high yield and throughput using the internal gelation process. Ann Nucl Energy 105:116–120. https://doi.org/10.1016/j.anucene.2017.03.010

50. Umbanhowar PB, Prasad V, Weitz DA (2000) Monodisperse emulsion generation via drop break off in a coflowing stream. Langmuir 16:347–351. https://doi.org/10.1021/la990101e

51. Than P, Preziosi L, Joseph D, Arney M (1988) Measurement of interfacial tension between immiscible liquids with the spinning rod tensiometer. J Colloid Interface Sci 124:552–559

52. Utada AS, Chu L-Y, Fernandez-Nieves A et al. (2007) Dripping, jetting, drops, and wetting: the magic of microfluidics. MRS Bull 32:702–708

53. Clanet C, Lasheras JC (1999) Transition from dripping to jetting. J Fluid Mech 383:307–326

54. Ambravaneswaran B, Phillips SD, Basaran OA (2000) Theoretical analysis of a dripping faucet. Phys Rev Lett 85:5332–5335

55. Ambravaneswaran B, Subramani H, Phillips S, Basaran O (2004) Dripping-jetting transitions in a dripping faucet. Phys Rev Lett 93. https://doi.org/10.1103/PhysRevLett.93.034501

56. Cramer C, Fischer P, Windhab EJ (2004) Drop formation in a co-flowing ambient fluid. Chem Eng Sci 59:3045–3058. https://doi.org/10.1016/j.ces.2004.04.006